

Dark-matter velocity dispersion in N-body simulations

Alvaro Domínguez^{1,2,3}

¹ Theoretische Physik, Ludwig-Maximilians-Universität, Theresienstr. 37, D-80333 München, Germany

² Laboratorio de Astrofísica Espacial y Física Fundamental, Apartado 50727, E-28080 Madrid, Spain

³ alvaro@theorie.physik.uni-muenchen.de

March 20, 2001

Abstract. The present work reports on a study of the spatially coarse-grained velocity dispersion in cosmological N-body simulations (OCDM and Λ CDM models) as a function of time ($z = 0-4$) and of the smoothing length ($0.6-20 h^{-1}$ Mpc). The main result is a polytropic relationship $\mathcal{I}_1 \propto \varrho^{2+\eta}$ between the coarse-grained peculiar kinetic energy density, \mathcal{I}_1 , and the coarse-grained mass density, ϱ , induced by the gravitational interaction. The “anomalous dimension” η , dependent on time and coarsening scale, is introduced as a compact measure of the deviations from the virial prediction $\eta_{\text{virial}} = 0$.

Key words: Gravitation; Methods: N-body simulations; (*Cosmology*:) large-scale structure of Universe

1. Introduction

Some recent works (Barbero et al., 1997; Buchert and Domínguez, 1998; Adler and Buchert, 1999; Domínguez et al., 1999; Buchert et al., 1999; Maartens et al., 1999; Domínguez, 2000) have explored theoretically a formulation of hydrodynamic kind for the nonlinear evolution of the gravitational instability and its application to the formation of large-scale structures. It intends to describe the dynamical evolution of the few most relevant fields (typically the coarse-grained mass density and velocity fields) in terms of a set of autonomous equations for those fields. This approach is to be compared with a mechanical formulation, describing the path of every particle, or with a kinetic formulation, focusing on the multiparticle distribution functions in phase space. An interesting result following from this hydrodynamic formulation are the corrections to the widely used dust model. These corrections arise from the nonlinear coupling to the structure below the smoothing length, which turn out to be relevant in the nonlinear regime (\leftrightarrow large density fluctuations about homogeneity). In fact, the corrected equations are generalizations of the adhesion model (Kofman and Shandarin, 1988; Gurbatov et al., 1989; Kofman et al., 1992; Melott et al., 1994; Sathyaprakash et al., 1995), which is known to reproduce quite well the gross features of the

structure evolved by gravitational instability in different cosmological scenarios. The hydrodynamic formulation requires the corrections to be expressed as functions of the coarse-grained mass density and velocity fields, so as to get a closed set of equations for these fields. This is, however, a major theoretical problem, since one cannot follow the standard procedure to close the hydrodynamic hierarchy by invoking “local thermal equilibrium” (Huang, 1987; Balescu, 1991): the ideas and the formalism of thermodynamics cannot be applied straightforwardly to a system dominated by its own gravity, this being in fact still an open question (see, e.g., the concise review by Hut (1997)).

In this work I report on the empirical search for closure relationships with the help of N-body simulations of large-scale structure formation. The results provided by the simulations can be fitted quite well by a “polytropic relationship”, borrowing the terminology from thermodynamics, between the smoothed mass density and the smoothed peculiar kinetic energy density, $\mathcal{I}_1 \propto \varrho^{2+\eta}$. This result supports the polytropic approximation used in the theoretical derivation of adhesion-like models (Buchert et al., 1999). The polytropic relationship improves with time, and so I conclude that it must be a consequence of the evolution by gravitational instability: in fact, for small coarsening lengths or large times, the exponent η is close to, but significantly smaller than the virial prediction following from the simple model of isolated, relaxed, structureless halos; thus, η can be termed an “anomalous dimension”.

The degree of anisotropy of the velocity dispersion (the departure from a spherically symmetric distribution of the dispersion) has also been studied, but in this case the scatter of the data is large and the results are not so conclusive. The anisotropy tends to decrease with increasing mass density (till a few percents at the largest probed densities), being however always larger than that associated to a Maxwellian distribution with the same density. This result speaks in favor of the approximation of isotropic velocity dispersion also employed in deriving adhesion-like models.

This work is organized as follows: in Sec. 2 I detail the method employed in the analysis of the simulations. Sec. 3 presents the results, which are discussed with the

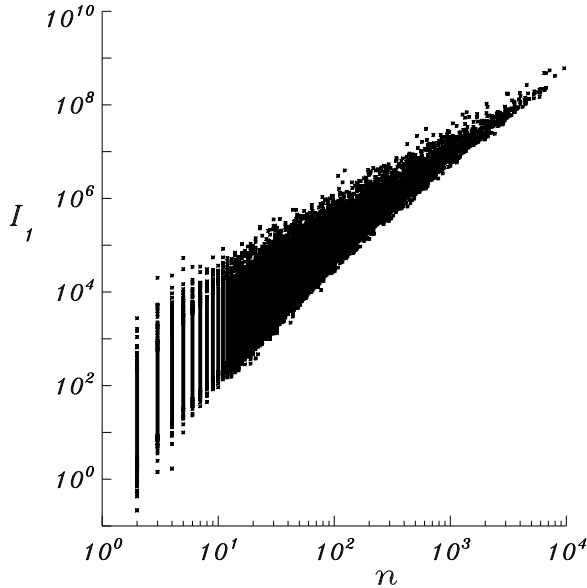


Fig. 1. Typical log-log scatter plot of the trace of the velocity dispersion tensor (in units of $\text{km}^2 \text{s}^{-2} (\text{Mpc}/h)^{-3}$, setting the particle mass $m = 1$) vs the number of particles. The data correspond to the Λ CDM model at redshift $z = 0$ with a smoothing length $L = 4.55 h^{-1}\text{Mpc}$.

help of theoretical arguments in Sec. 4. Finally, a brief mathematical discussion of some topics required in the main text are collected in the Appendix.

2. Method

The analyzed CDM simulations were performed by *The Hydra Consortium* (Couchman et al., 1995) using the *AP³M* algorithm. They consist of a cubic box (periodic boundary conditions) of side length $100 h^{-1}\text{Mpc}$ at the present epoch, containing $N = 86^3$ particles. Two different cosmological models have been considered, OCDM ($\Omega_m = 0.3$, $\Omega_\Lambda = 0.0$, $h = 0.81$, $\sigma_8 = 1.06$, $\Gamma = 0.25$, $m = 1.63 \times 10^{11} M_\odot$) and Λ CDM ($\Omega_m = 0.3$, $\Omega_\Lambda = 0.7$, $h = 0.96$, $\sigma_8 = 1.22$, $\Gamma = 0.25$, $m = 1.37 \times 10^{11} M_\odot$), at three times, corresponding to redshifts $z = 0, 1.4, 3.6$.

The hydrodynamic formulation can be derived by means of a coarsening procedure (Domínguez, 2000). Given a comoving smoothing scale L , the coarse-grained mass density, velocity and velocity dispersion fields are defined respectively as follows:

$$\varrho(\mathbf{x}, t) = \frac{m}{[a(t)L]^3} \sum_{\alpha=1}^N W\left(\frac{\mathbf{x} - \mathbf{x}_\alpha}{L}\right),$$

$$\varrho \mathbf{u}(\mathbf{x}, t) = \frac{m}{[a(t)L]^3} \sum_{\alpha=1}^N \mathbf{u}_\alpha(t) W\left(\frac{\mathbf{x} - \mathbf{x}_\alpha}{L}\right), \quad (1)$$

$$\Pi(\mathbf{x}, t) = \frac{m}{[a(t)L]^3} \sum_{\alpha=1}^N [\mathbf{u}_\alpha(t) - \mathbf{u}(\mathbf{x}, t)] [\mathbf{u}_\alpha(t) - \mathbf{u}(\mathbf{x}, t)] W\left(\frac{\mathbf{x} - \mathbf{x}_\alpha}{L}\right).$$

(Π is a second-rank tensor). Here, $a(t)$ denotes the expansion factor, m is the mass of a particle, \mathbf{x}_α and \mathbf{u}_α represent the comoving position and peculiar velocity, respectively, of the α -th particle, and $W(\cdot)$ is a (normalized) smoothing window.

Starting from the coordinates $\{\mathbf{x}_\alpha, \mathbf{u}_\alpha\}_{\alpha=1\dots N}$ provided by the simulation, the definitions (1) were implemented with a cubic top-hat window,

$$W(\mathbf{z}) = \theta(1 - 2|z_1|) \theta(1 - 2|z_2|) \theta(1 - 2|z_3|), \quad (2)$$

where $\theta(\cdot)$ is the step function. In total 13 different values of L were explored, spanning the range from $0.6 h^{-1}\text{Mpc}$ up to $20 h^{-1}\text{Mpc}$ and equally separated in a logarithmic scale. For each value of L , a minimum (corresponding to the largest L) of 2×10^4 randomly centered, non empty coarsening cells were probed.

The velocity dispersion tensor $\Pi_{ij}(\mathbf{x})$ was studied as a function of the density $\varrho(\mathbf{x})$, or equivalently, of the number of particles contained in the cell at \mathbf{x} , namely $n(\mathbf{x}) = [(aL)^3/m]\varrho(\mathbf{x})$. For the purposes of this work, it sufficed to consider the three eigenvalues λ_i of the tensor Π , or better, its three principal scalar invariants:

$$\mathcal{I}_1 = \text{tr } \Pi = \lambda_1 + \lambda_2 + \lambda_3,$$

$$\mathcal{I}_2 = \frac{1}{2} [(\text{tr } \Pi)^2 - \text{tr}(\Pi : \Pi)] = \lambda_1 \lambda_2 + \lambda_2 \lambda_3 + \lambda_3 \lambda_1,$$

$$\mathcal{I}_3 = \det \Pi = \lambda_1 \lambda_2 \lambda_3. \quad (3)$$

The quantity $(1/2)\mathcal{I}_1$ is the peculiar kinetic energy per unit volume due to the motion of the particles relative to the cell center of mass. The quantity $p = (1/3)\mathcal{I}_1$ thus corresponds to a kinetic pressure. The other two invariants can be related to the degree of anisotropy of the tensor Π . More precisely, the dimensionless coefficients

$$\alpha = 1 - \frac{3\mathcal{I}_2}{\mathcal{I}_1^2}, \quad \beta = 1 - \frac{27\mathcal{I}_3}{\mathcal{I}_1^3}, \quad (4)$$

quantify the departure from the isotropic case, $\lambda_1 = \lambda_2 = \lambda_3 = p$. I show in the Appendix that $0 \leq \alpha, \beta \leq 1$, and they vanish if and only if Π is isotropic. Moreover, it follows from its definitions that $\beta \approx 3\alpha$ for small anisotropy.

To check that this smoothing algorithm was right, it was applied to an ideal gas simulation. The results for the dependence of the kinetic pressure p and the anisotropy parameters α, β on n agree with the predicted relationships (see the Appendix).

In the next Section I also discuss how the results depend on the smoothing details (e.g., on the choice of the window (2)). I anticipate that the conclusions to be extracted are robust.

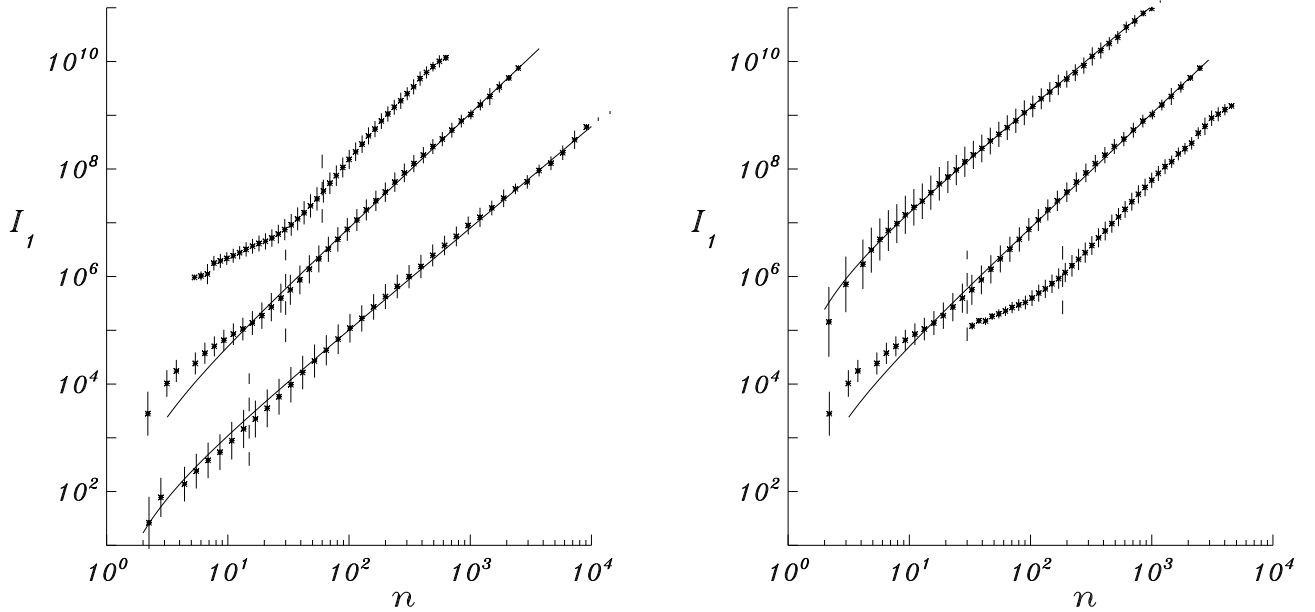


Fig. 2. Binned log-log plot of the trace of the velocity dispersion tensor (same units as Fig. 1) vs the number of particles for the Λ CDM model. The error bars correspond to the estimated $1\text{-}\sigma$ variance. On the left, for three redshifts (from top to bottom, $z = 0, 1.4, 3.6$) at a fixed smoothing length $L = 4.55 h^{-1}\text{Mpc}$. On the right, for three smoothing scales (from top to bottom, $L = 1.41, 4.55, 8.33 h^{-1}\text{Mpc}$) at a fixed redshift $z = 1.4$. The solid line corresponds to the fit (6), and the dashed line marks n_c , Eq. (5).

3. Results

The results concerning the three invariants as a function of the particle number are qualitatively the same in the whole range of smoothing scales and times explored, and for the two cosmological models Λ CDM and Λ CDM. Fig. 1 is a typical example of a \mathcal{I}_i vs n scatter plot. The data suggest a polytropic relationship between the scalar invariants and n , more and more accurate for larger n . Hence, it appears that the increasingly larger scatter for smaller particle numbers is mainly due to the discrete character of the variable n . To eliminate this noise, the log-log plots of the raw data were binned into 40 subintervals on the n -axis: this effectively means averaging the scalar invariants for different fixed values of n and provides also an estimate of the variance. This scatter is in fact the main source of error in the parameters η and κ of the fit (6). Fig. 2 collects a set of representative cases after implementation of this procedure, where the advocated polytropic dependence is evident. To be sure that this averaging method does not introduce artificial features, the analysis was repeated by varying the number of bins, from 10 up to the limiting case in which each possible value of the discrete variable n is treated as a bin. The conclusions are robust and the results do not depend on the amount of binning. (Changes of the number of bins within this range induce variations in the best-fit parameters η and κ which are well within

the error region in Fig. 4). The choice of 40 bins is a good compromise that efficiently discards the noise but still preserves the relevant features of the \mathcal{I}_i - n relationship.

Another check probed the influence of the choice of smoothing window. Since the eigenvalues λ_i are the sum of a large number of positive contributions, that is, they are “extensive quantities”, it can be expected that they will be rather insensitive to the details of the window boundary. And indeed this is so, the only difference being a consequence of the discrete nature of n . Fig. 3 shows the typical result after using three different smoothing windows: a cubic top-hat, Eq. (2), a spherical top-hat, $W(\mathbf{z}) = \theta(1 - (4\pi/3)^{1/3}|\mathbf{z}|)$, and a Gaussian, $W(\mathbf{z}) = \exp(-\pi|\mathbf{z}|^2)$. The windows are normalized to unity and give the same weight (=1) to the origin: the comparison is then straightforward. The cubic and spherical top-hat windows yield indistinguishable results, demonstrating that window anisotropy is not relevant (this could also be expected, see the last paragraph in this Sec.). The Gaussian smoothing also gives similar results, but now a slight difference in the small- n end is observed, because the discreteness of n implies (i) that $\Pi = 0$ if $n = 1$ for the top-hat windows and (ii) that for small n , Π is dominated by far contributions from the Gaussian tails. However, as discussed later, the discreteness constraint $\Pi = 0$ if $n = 1$ for a top-hat window can be taken into account in a simple manner and indeed the polytropic fit (6) holds very

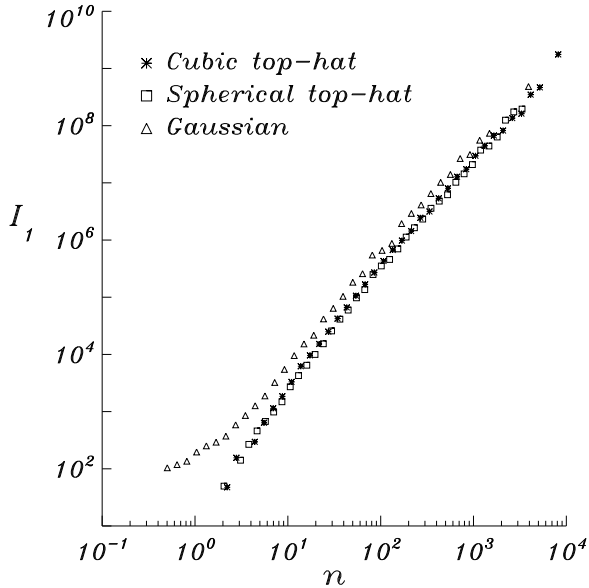


Fig. 3. Log-log plot of the trace of the velocity dispersion tensor vs the number of particles, computed with three different smoothing windows. The data correspond to the Λ CDM model, $z = 0$, $L = 3.45 h^{-1}\text{Mpc}$.

well even for $n \sim 1$. Hence, the cubic top-hat window was selected, because it is also most easily implemented.

A final check, carried out only for the particular time $z = 0$, was to restrict the coarsening procedure to a sub-volume of the simulation box (1/64 of the total volume), so as to find out to what extent the results are exclusive of the simulation volume of $100 h^{-1}\text{Mpc}$ side length: as expected, the quality of the fits are slightly worse because of the reduced number of particles, but the conclusions remain the same.

As exemplified by Fig. 2, one finds a well defined relationship between \mathcal{I}_1 and n , in which three different behaviors can be identified: a polytropic dependence $\mathcal{I}_1 \propto n^{2+\eta}$ for n larger than a certain value n_c , a bending upwards for $1 < n < n_c$, and finally a bending downwards for n close to 1 (due to the constraint $\Pi = 0$ if $n = 1$). The value of n_c increases with the redshift and the smoothing length. An estimate of the function $n_c(L, z)$ is given by

$$n_c = F(z)\bar{n}_L, \quad \bar{n}_L := (86 L/100)^3. \quad (5)$$

\bar{n}_L is the average particle number in a cell of comoving side length L ($h^{-1}\text{Mpc}$), and $F(z)$ is a mild function of the redshift, $F = 1$ for a redshift $z = 3.6$ and decreases slowly for smaller z ($F = 0.25$ for $z = 0$). This fit for $n_c(L, z)$ is conservative in the sense of slightly overestimating n_c as L decreases, however it is precise enough: Fig. 2 shows that the polytropic fit is in fact still well followed by the data for a certain range below the chosen n_c . The best-fit parameters η and κ in Eq. (6) are quite insensitive to the

precise value of n_c . The intermediate range $1 < n < n_c$ contains underdense regions (n_c corresponds to a density contrast $\delta_c = F(z) - 1$); the deviations from the polytropic fit may then be a consequence of the shear induced by the surrounding dense regions¹. Nonetheless, this failure of the polytropic relationship is unimportant, being restricted to ever smaller density contrasts ($\delta_c \approx -0.75$ at $z = 0$).

The binned data in the range $n > n_c$ were fitted to the polytropic relationship

$$\mathcal{I}_1 = \frac{m}{(aL)^3} \kappa (n - 1)^{2+\eta}. \quad (6)$$

The exponent η can be called an “anomalous dimension”, since it represents the departure from the virial (\sim mean-field) prediction (see Sec. 4). The factor $n - 1$ enforces the discreteness constraint $\mathcal{I}_1 = 0$ for $n = 1$. This improves the fit on the small- n region in the cases that it extends down to $n \sim 1$ and it is also suggested by the simulated ideal gas: the ideal gas pressure-density relation is still obeyed with the replacement $n \rightarrow n - 1$ when the smoothing length is so small that most of the coarsening cells contain just a few particles. The parameters η and κ were determined by the least-squares method. The fit was carried out only when the fit range in n spanned at least a decade (in which case the range in \mathcal{I}_1 always extends over at least two decades); the polytropic fit is still consistent when this condition is not met, but the large errors deprive it of significance. In the best cases, the fit range in n included three decades. The time and smoothing-length dependences of the parameters η and κ for the Λ CDM model are plotted in Fig. 4. The results for the OCDM model are very close.

The other two invariants, \mathcal{I}_2 and \mathcal{I}_3 , are also fitted by a polytropic dependence. In fact, it turns out that the anisotropy parameters α and β computed with the fitting functions are extremely small and n -independent. The reason is that the binned (=averaged) velocity dispersion, being only a function of the scalar n , must be isotropic. The anisotropy parameters must be calculated for the raw data, before binning: Fig. 5 shows a typical α vs n scatter plot. The plots of the parameter β look similar (in fact, the relation $\beta \approx 3\alpha$ is a very good approximation already for $\alpha \sim 0.1$: then, one should rather study, e.g., $\beta - 3\alpha$ to gain non-redundant information). Apart from the large scatter for small particle number due to the discreteness of n , there is also an important dispersion even for large n , because the anisotropy must be determined by something else than only a scalar. Moreover, unlike the “extensive” scalar invariants, the anisotropy parameters, being essentially the difference between eigenvalues, Eq. (A.2), are more sensitive to the discreteness of n . Thus, the data quality just allows to confirm that α and β tend to decay with increasing n but to remain somewhat larger than the average ideal gas anisotropy, $\alpha_{\text{ideal}} \approx 5/(3n)$ (see the Ap-

¹ I am grateful to M. Kerscher for this remark.

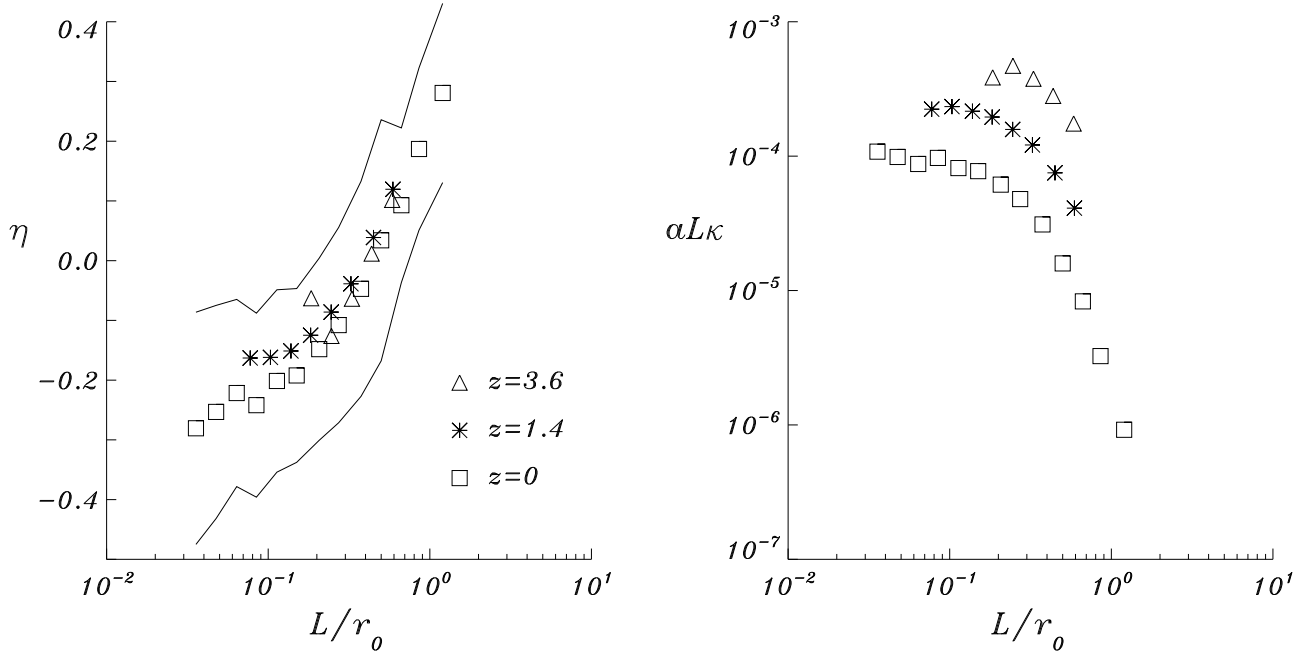


Fig. 4. Plot of the best-fit parameters in Eq. (6) vs the smoothing length for the Λ CDM model at the three times studied. r_0 is the scale of nonlinearity, Eq. (7). The two lines delimit the estimated 1- σ error region. The error bars for κ are about the same size as the plot symbols. The virial prediction reads $\eta = 0$ and $aL\kappa = L$ -independent.

pendix). No significant dependence (if any) with time and smoothing length could be detected.

4. Discussion and Conclusion

The simulations show a clear evidence for a polytropic relationship (6) between the density and the scalar invariants of the velocity dispersion tensor. The fits improve with decreasing redshift or smoothing scale; hence one is lead to view them as a general consequence of the evolution by gravitational instability. In agreement with this interpretation, this relationship occurs for both the Λ CDM and the OCDM models. Thus, it seems that the existence of the polytropic dependence itself is independent of the background cosmological model, which would perhaps only affect the values of the fitting parameters slightly.

The theoretical explanation of the precise values of the fitting parameters is not evident. Fig. 4 shows that the function $\eta(L, z)$ can be approximately written in fact as a function of the single variable $L/r_0(z)$, where $r_0(z)$ is the scale of nonlinearity, defined by the condition

$$\frac{\langle (n - \bar{n}_L)^2 \rangle}{\bar{n}_L^2} = 1, \quad \text{for } L = r_0. \quad (7)$$

The Λ CDM simulation provides the values $r_0 = 3.2, 7.7, 16.7 h^{-1}$ Mpc, respectively for the three considered redshifts. This property agrees nicely with the evolution by gravitational instability in a hierarchical scenario. The

points for $\kappa(L, z)$ can be made to collapse on a single curve too if κ is also suitably rescaled by a z -dependent factor; but this must be viewed as pure phenomenology, since no theoretical explanation for the values of this rescaling factor could be given.

A theoretical argumentation by Buchert and Domínguez (1998) provides a polytropic relationship with a fixed $2 + \eta = 5/3$: this is equivalent to the adiabatic evolution of an ideal gas and was justified for early times and under restrictive initial conditions. However, Fig. 4 shows that, precisely in the opposite limit of nonlinear scales/large times ($L < r_0$), η is close to this “adiabatic value”, which even seems to be an asymptote. But the errors are too large and the probed range of nonlinear lengths too narrow to draw a firm conclusion.

This flattening of $\eta(L)$ suggests another possible explanation of the polytropic relationship. It seems sensible to hypothesise that, for smoothing lengths L well in the nonlinear regime, the kinetic energy should be fixed by the virial theorem: if the coarsening cells can be idealized as virialized, structureless halos, then $(aL)^3 \mathcal{I}_1$ should be proportional to the potential gravitational energy of the coarsening cell, which could in turn be estimated as $\sim G(mn)^2/aL$. This implies immediately a polytropic dependence (6) with $\eta_{virial} = 0$ and $\kappa_{virial} \propto (aL)^{-1}$. This idealized model was employed to simulate scatter plots as Fig. 1: the same distribution of particle numbers n but with \mathcal{I}_1 randomly drawn from the condition that the differences $\mathbf{u}_\alpha - \mathbf{u}$ in the definition (1) of Π are independent,

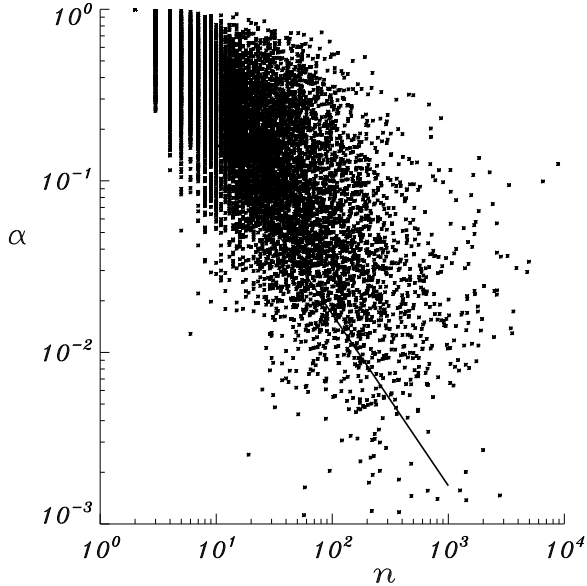


Fig. 5. Typical log-log scatter plot of the anisotropy parameter α vs the particle number. The data correspond to the Λ CDM model, $z = 0$, $L = 4.55 h^{-1}\text{Mpc}$. The solid line represents the average anisotropy for a Maxwellian distribution.

Gaussian distributed random variables with zero mean and a variance given by the virial theorem. In this way, a estimated error $< 2 \cdot 10^{-3}$ for η_{virial} was gained. Fig. 4 shows that the best-fit values of η and κ are close to the virial predictions for small L , but the deviations, in particular those of η , lie above the $1\text{-}\sigma$ level.

The reason for this discrepancy must lie on the assumptions involved: (i) the potential energy should be dominated by the contribution from the structure on the scale L and (ii) each coarsening cell should be approximately isolated and in a relaxed, stationary state, so that the virial theorem holds. The long-range nature of gravity could perhaps justify assumption (i) even in a hierarchical scenario, when the matter distribution is far from smooth inside the coarsening cells, provided it is not too diluted either on the scale L . But it cannot be excluded that the corrections due to the substructure contribute significantly to the discrepancy. Assumption (ii) can be easily violated: the coarsening cells may have a significant interaction with neighboring cells, or be part of a larger virialized halo or contain a bunch of streaming particles far from any (quasi-)stationary state. As evidence, consider Fig. 3 in (Knebe and Müller, 1999): it is equivalent to my \mathcal{I}_1 - n plots but the points correspond to groups determined by a friends-of-friends algorithm, rather than by coarsening boxes of fixed side length. What Knebe and Müller identify as unvirialized groups clearly tend to yield a negative η , in agreement with the trend observed in Fig. 4. There-

fore, a very interesting result is that these violations of the “virialized halo” conditions (i-ii) do not destroy the polytropic relationship itself predicted by the virial theorem, but only change the values of the parameters.

Finally, in (Domínguez, 2000) I propose the following expression for the velocity dispersion tensor:

$$\Pi_{ij} \propto \varrho(\partial_k u_i)(\partial_k u_j). \quad (8)$$

It is derived from a simple estimate of the difference $\mathbf{u}_\alpha - \mathbf{u}$ in the definition of Π , Eq. (1), and the scale L is assumed to be well in the nonlinear regime. In fact, if the smoothing length is taken within the linear regime ($L > r_0$), one can estimate $|\partial_k u_i| \sim |\nabla \cdot \mathbf{u}| \propto |\delta|$ and hence $\mathcal{I}_1 \sim n(n - \bar{n}_L)^2$: obviously, the plots in Fig. 2 do not look at all like this prediction. This has an easy explanation: Π is essentially an “extensive” quantity which probes the scales smaller than the smoothing length L . Thus, when L belongs to the linear regime, Π must be rather given by a dominant correction to the estimate (8) from the small scales, since the linear scales carry comparatively too little peculiar kinetic energy. Comparison with the results for nonlinear L is not possible without an estimate of $|\partial_k u_i|$. But since the interaction between neighbor cells is inherent to the derivation of Eq. (8), one may wonder that it could provide the explanation of the nonvanishing anomalous dimension for small L .

In conclusion, N-body simulations have provided evidence for a polytropic relationship between the coarse-grained mass density and peculiar kinetic energy fields. I have introduced the anomalous dimension η as a simple measure of the (scale and time dependent) departures from a “virialized halo” state. It was found that, for smoothing lengths well in the nonlinear regime, η is significantly smaller than zero. There still remains the task of theoretically explaining this polytropic dependence and the precise values of the anomalous dimension as a function of time and scale.

Appendix A: The anisotropy parameters α and β

In this Appendix I derive some properties of the anisotropy parameters defined in Eqs. (4). The non-negativity of the eigenvalues, $\lambda_i \geq 0$, implies the bounds $0 \leq \alpha, \beta \leq 1$. In fact, $\mathcal{I}_i \geq 0$ yields immediately that $\alpha, \beta \leq 1$. On the other hand, for any triplet of non-negative numbers, the following inequalities hold (Abramowitz and Stegun, 1965):

$$\begin{aligned} \sum_{i=1}^3 \lambda_i^2 &\geq \lambda_1 \lambda_2 + \lambda_2 \lambda_3 + \lambda_3 \lambda_1, \\ \frac{1}{3} \sum_{i=1}^3 \lambda_i &\geq (\lambda_1 \lambda_2 \lambda_3)^{1/3}, \end{aligned} \quad (\text{A.1})$$

and the equality is satisfied if and only if all three numbers are equal. Combining these inequalities with the defini-

tions (3-4), it is found that α and β must be non-negative, and they are zero if and only if the tensor Π is isotropic.

Let us write $\lambda_i = \frac{1}{3}\mathcal{I}_1 + \delta\lambda_i$, so that the coefficients $\delta\lambda_i$ represent the deviation from isotropy and satisfy $\sum_i \delta\lambda_i = 0$. Then:

$$\alpha = -\frac{3}{\mathcal{I}_1^2} \sum_{i < j} (\delta\lambda_i)(\delta\lambda_j), \quad (\text{A.2})$$

$$\beta = 3\alpha - \frac{27}{\mathcal{I}_1^3} (\delta\lambda_1)(\delta\lambda_2)(\delta\lambda_3),$$

and in the limit of small anisotropy, $|\delta\lambda_i| \ll \mathcal{I}_1$, the equality $\beta \approx 3\alpha$ holds.

The simulations of the ideal gas provide $\langle \alpha_{\text{ideal}} \rangle_n \approx 5/(3n)$ with a large scatter, for the reason discussed towards the end of Sec. 3 ($\langle \dots \rangle_n$ refers to the binning procedure detailed in that Sec.). Nevertheless, this result is reliable because the $1/n$ dependence can be easily explained: Π for a coarsening cell containing n particles is the sum of n independent random variables. Hence, for not too small n , the average $\langle \Pi \rangle_n$ will be isotropic and extensive, with the scaling $\mathcal{I}_1 \sim n$, while fluctuations around isotropy will scale like $\delta\lambda \sim \sqrt{n}$. Expression (A.2) then yields that $\alpha \sim 1/n$.

Acknowledgements. The author is grateful to P. A. Thomas for providing the simulations data, and to C. Beisbart, T. Buchert, R. Domínguez-Tenreiro, M. Kerscher, P. A. Thomas and R. Trasarti-Battistoni for their useful comments on this work.

References

- Abramowitz, M. and Stegun, I. A. (eds.), 1965, Handbook of mathematical functions, pp 10–11, Dover Publications, New York
- Adler, S. and Buchert, T., 1999, A&A 343, 317
- Balescu, R., 1991, Equilibrium and Non-equilibrium Statistical Mechanics, John Wiley & Sons
- Barbero, J. F., Domínguez, A., Goldman, T., and Pérez-Mercader, J., 1997, Europhys. Lett. 38, 637
- Buchert, T. and Domínguez, A., 1998, A&A 335, 395
- Buchert, T., Domínguez, A., and Pérez-Mercader, J., 1999, A&A, 349, 343
- Couchman, H. M. P., Thomas, P. A., and Pearce, F. R., 1995, ApJ 452, 797
- Domínguez, A., 2000, Phys. Rev. D 62, 103501
- Domínguez, A., Hochberg, D., Martín-García, J. M., Pérez-Mercader, J., and Schulman, L. S., 1999, A&A 344, 27; Erratum: A&A 363, 373
- Gurbatov, S. N., Saichev, A. I., and Shandarin, S. F., 1989, MNRAS 236, 385
- Huang, K., 1987, Statistical Mechanics, John Wiley & Sons
- Hut, P., 1997, Complexity 3(1), 38
- Knebe, A. and Müller, V., 1999, A&A 341, 1
- Kofman, L., Pogosyan, D., Shandarin, S. F., and Melott, A. L., 1992, ApJ 393, 437

- Kofman, L. A. and Shandarin, S. F., 1988, Nature 334, 129
- Maartens, R., Triginer, J., and Matravers, D. R., 1999, Phys. Rev. D 60, 103503
- Melott, A. L., Shandarin, S. F., and Weinberg, D. H., 1994, ApJ 428, 28
- Sathyaprakash, B. S., Sahni, V., Munshi, D., Pogosyan, D., and Melott, A. L., 1995, MNRAS 275, 463